Published in final edited form as:
Angiogenesis. 2014 October ; 17(4): 823–830. doi:10.1007/s10456-014-9436-3.

VEGF neutralization can prevent and normalize arteriovenous malformations in an animal model for hereditary hemorrhagic telangiectasia 2

Chul Han[#1], **Se-woon Choe**[#1,2], **Yong Hwan Kim**[1], **Abhinav P. Acharya**[3], **Benjamin G. Keselowsky**[3], **Brian S. Sorg**[3], **Young-Jae Lee**[4], and **S. Paul Oh**[1,4,*]

[1] Department of Physiology and Functional Genomics, College of Medicine, University of Florida, Gainesville, FL 32610

[2] Department of Biomedical Engineering, Tongmyong University, Busan, Republic of Korea

[3] J. Crayton Pruitt Family Department of Biomedical Engineering, College of Engineering, University of Florida, Gainesville, FL 32611

[4] World Class University program, Lee Gil Ya Cancer and Diabetes Institute, Gachon University of Medicine and Science, Incheon, Republic of Korea

[#] These authors contributed equally to this work.

Abstract

Arteriovenous malformation (AVM) refers to a vascular anomaly where arteries and veins are directly connected through a complex, tangled web of abnormal AV fistulae without a normal capillary network. Hereditary hemorrhagic telangiectasia (HHT) types 1 and 2 arise from heterozygous mutations in endoglin (*ENG*) and activin receptor-like kinase 1 (*ALK1*), respectively. HHT patients possess AVMs in various organs, and telangiectases (small AVMs) along the mucocutaneous surface. Understanding why and how AVMs develop is crucial for developing therapies to inhibit the formation, growth, or maintenance of AVMs in HHT patients. Previously, we have shown that secondary factors such as wounding are required for *Alk1*-deficient vessels to develop skin AVMs. Here we present evidences that AVMs establish from nascent arteries and veins rather than from remodeling of a preexistent capillary network in the wound-induced skin AVM model. We also show that VEGF can mimic the wound effect on skin AVM formation, and VEGF neutralizing antibody can prevent skin AVM formation and ameliorate internal bleeding in *Alk1*-deficient adult mice. With topical applications at different stages of AVM development, we demonstrate that the VEGF blockade can prevent the formation of AVM and cease the progression of AVM development. Taken together, the presented experimental model is an invaluable system for precise molecular mechanism of action of VEGF

[*] Correspondence: S. Paul Oh, Ph.D. Department of Physiology and Functional Genomics University of Florida College of Medicine P.O. Box 100274 1600 SW Archer Road, Room CG-20B Gainesville, FL 32610 Phone: 352-273-8232 Fax: 352-864-0270 ohp@ufl.edu.

Author Contributions

C.H. and S.W.C performed the experiments and analyzed data and wrote manuscript. Y.H.K. and Y.J.L. performed experiments. A.P.A. and B.G.K provided PLGA particles, and B.S.S. supervised the window chamber experiments. S.P.O. designed experiments, supervised entire project, and edited manuscript, which was accepted by all co-authors.

The authors have declared that no conflict of interest exists.

blockades as well as for preclinical screening of drug candidates for epistaxis and gastrointestinal bleedings.

Introduction

Hereditary hemorrhagic telangiectasia (HHT) is an autosomal dominant vascular disorder, characterized by spontaneous recurrent epistaxis, mucocutaneous telangiectasia, and AVMs in the brain, lung, liver or GI tract [1, 2]. Two major types 1 and 2 HHT arise from mutations in endoglin (*ENG*) and activin receptor-like kinase 1 (ACVRL1; ALK1), respectively [3, 4]. While cerebral and pulmonary AVMs are generally believed to arise during fetal development or neonatal periods [5], small AVMs called telangiectasia forming in mucocutaneous layers, such as eye lid, lips, tongue and nasal cavity mostly develop during post-developmental stages [1]. Therefore, therapeutic window for prevention of mucocutaneous telangiectasia is open for adult HHT patients.

Epistaxis is the most common symptom of HHT, mostly due to the rupture of telangiectases formed in the nasal mucosa. The frequency and severity of epistaxis increase by age as more than 90% of HHT patients over 65 years old exhibit moderate to severe epistaxis [6]. Recently, a growing number of case reports demonstrated bevacizumab (VEGF-neutralizing antibody) is effective for epistaxis in HHT patients [7-10]. In those studies, the final output was epistaxis severity score (ESS) [11] i.e., frequency, duration, and amount of nose bleeding, hemoglobin level and the number of blood transfusion before and after the treatment. However, there has been no direct demonstration how the VEGF blockade affects the formation and/or maintenance of AVMs and how it is related to the improvement of ESS.

Using inducible *Alk1* knockout mice, we have previously demonstrated that development of AVMs in mucocutaneous layer requires a ‘second hit’ such as wounding, in addition to *Alk1*-deficiency [12, 13]. This result infers that blockage of the second hit could be a therapeutic strategy for inhibiting AVM formation. Here we show that development of *de novo* mucocutaneous AVMs involves growth of nascent blood vessels, and that angiogenic stimulation is a key factor in the wound responses as a second hit. In addition, we show direct *in vivo* evidence that VEGF blockade not only inhibits the initiation of AVMs but also can normalize established AV shunts. These results provide a better scientific basis for the therapeutic effect of VEGF blockades for epistaxis and GI bleeding in HHT patients.

Results and Discussion

The origin and process of AVM development are poorly understood. A current view is that detrimental factors such as oxidative stresses may lead to the regression of preexisting AV connecting capillaries, and that persistent vessels from the regression in turn develop into AV fistulae [14]. A study with an *alk1* mutant zebrafish model has shown that retention of transient arteriovenous connections underlie cranial AV shunts [15]. The intravital hyperspectral imaging system with dorsal window chamber on *Alk1*-deficient, wound-induced AVM model allows monitoring levels of hemoglobin (Hb) oxygen saturation during vascular remodeling in response to wound. Thus, it is a unique tool to distinguish blood

vessels containing arterial from venous bloods and to observe the birth, progression, and remodeling of AV shunts[12, 16, 17].

Figure 1 shows daily bright-field and spectral images of vascular remodeling 2-7 days after wound-infliction and tamoxifen injection (day 0) on a $R26^{CreER/+}$;$Alk1^{2f/2f}$ mouse. Entire course of lower magnification whole-window views of the same mouse (**Figure S1**) and two control mice ($R26^{+/+}$;$Alk1^{2f/2f}$; **Figure S2-5**) are also presented. Four AV shunts (AV1-AV4) are indicated (**Figure 1, Figures S6** and **S7**). AV1 constitutes one feeding artery and multiple draining veins (**Figure 1D**). On day 2, the adjacent artery and vein had thickened tips (**Figure 1A**), and the AV shunt seemed to be established by day 3 as the arterial blood flowed into the venous side (**Figure 1B inset**). The AV connection became clearer in the bright field image of the following day with dilatation of the vein connected to the artery (**Figure 1C**). The AVM structure emerged on day 5 as the AV shunts passed through multiple venous anastomoses (**Figure 1D**). AV2 and AV3 demonstrate the examples of AV shunt formations from distant arteries and veins. Peculiar growth of a venous vessel toward the AV1 complex from day 4 resulted in AV shunt by day 6 (AV2; **Figure 1C-E**). Similar growth of an arterial branch toward a venous branch resulted in an AV shunt by day 5 (AV3; **Figure 1B-E**). A similar but simpler AV shunt than AV1 established between an adjacent artery and vein is shown in AV4 (**Figures S6** and **S7**). A shunt between this artery and vein was initiated on days 2-3, and the clear morphological connections were shown on subsequent days. These data suggest that AV shunts develop from newly established connections between arteries and veins – whether adjacent or distant – during active angiogenesis rather than from the remodeling of preexisting AV connections in this wound-induced AVM model.

The looping structure of AV shunts appeared in the wound-induced adult skin AVM model (e.g. AV1 and AV4) is remarkably similar to the looping morphology of AV shunts developed in the brain and lungs of neonatal *Alk1* mutant model [12], suggesting a common etiology between these two models. However, the extent to which the AVM model found in *Alk1* mutants can extrapolate into the mechanism of other AVMs remains to be investigated.

In order to test whether angiogenic or inflammatory stimulation plays a crucial role for the wound response in *de novo* AVM formation of the *Alk1*-iKO [Tamoxifen (TM) injected $ROSA26^{CreER/+}$;$Alk1^{2f/2f}$ adult] model [12], we first examined if VEGF or lipopolysaccharides (LPS) can mimic the wound effect on the formation of AVM. VEGF, LPS or PBS encapsulated in PLGA [Poly (d,l lactide-co-glycolide)] [18, 19] was subcutaneously implanted on the tamoxifen injected control ($R26^{+/+}$;$Alk1^{2f/2f}$) or *Alk1*-iKO mice without wounding. After 9 days, the latex dye was infused through the left heart to visualize the blood vessels. Since the latex dye does not traverse to capillary beds unless an AV shunt is present, latex dye injection is a reliable tool to confirm the presence of AV shunts [12].

In VEGF- or LPS-PLGA-injected control mice, a higher vascular density was evident around the particle-injected areas compared to uninjected areas of the same mouse, but AV shunts were not observed (**Figure 2A** and **2B**). PBS-PLGA particles occasionally induced higher vascular densities around implantation sites in *Alk1*-iKO mice but did not result in

apparent vascular malformation (**Figure 2C**). In the VEGF-PLGA-implanted *Alk1*-iKO skin, however, tortuous, irregular, and excessive blood vessels were developed around the particles, and the dilated draining veins contained latex dye, demonstrating the presence of AV shunts (**Figure 2DF**). LPS-PLGA also mimicked the wounding, comparable to VEGF-PLGA (**Figure 2G**). Since LPS can induce angiogenesis [20-22], we tested if angiogenesis is also a key event in LPS-stimulated AVM formation. As shown in **Figure 2I**, VEGF-neutralizing antibody (G6.31) treatment [23, 24] could block AVM formation by LPS in *Alk1*-iKO mice. Taken together, these results suggest that angiogenesis is a critical element among the wound responses for inducing AVM formation in *Alk1*-deficient blood vessels.

This result is consistent with *de novo* brain AVM formation by viral delivery of VEGF and Cre into $Alk1^{2f/2f}$ brain [13]. In this brain AVM model, bevacizumab treatment could block AVM development [25]. Since AVM was induced by VEGF in this model, however, it confirmed that VEGF is a specific AVM inducer in this model, but the inhibitory effect of the VEGF-blockade may be limited for 'VEGF-induced' AVMs. To test whether a VEGF blockade can inhibit the development of wound-induced AVM formation, wounded *Alk1*-iKO mice were treated with G6.31 or saline (or IgG). Control *Alk1*-iKO mice exhibited typical AV shunts with excessive, tortuous, and dilated vessels surrounding the wound (**Figure 3A-C** and **Figure S8AC**). In contrast, AV shunts were rarely observed in G6.31-treated animals and there were fewer tortuous and irregular vessels near the wound (**Figure 3D-F** and **Figure S8D-F**). Area covered by blood vessels containing the latex dye in a given area was used as an index of AVM formation [12]. The G6.31-treated group displayed about 40% reduction in latex dye-containing vessel area compared to the control group (21.2 % versus 34.6 %, respectively) (**Figure 3G**). This result demonstrates that G6.31can effectively inhibit the formation of AVMs in *Alk1*-deficient subdermal vessels responding to wounding.

Alk1-iKO mice die within 2-3 weeks after tamoxifen treatment with severe hemorrhages in the lung and GI tract [12]. Since naturally occurring AVMs in these organs of *Alk1*-iKO mice are the major cause of bleeding, we examined whether G6.31 treatment suppresses internal bleeding. Hemoglobin levels of *Alk1*-iKO mice treated with saline was about 8.6 g/dl, while those with G6.31 appear to be near the normal hemoglobin level (mean: 13.8 g/dl) (**Figure 3H**). Consistently, hemorrhagic signs were rarely observed in the G6.31-treated groups upon visual inspections of thoracic and abdominal organs. The saline-treated *Alk1*-iKO mice showed moderate to severe bleeding in the lungs and GI tract whereas the majority of the G6.31-treated group displayed none to weak GI and lung hemorrhage (**Figure 3I**). *Alk1*-iKO mice exhibit enlargement of heart due to hemorrhages. Such a cardiomegaly phenotype was significantly attenuated in the G6.31-treated group, compared with the saline-treated group (**Figure 3J**).

Based on the window chamber images, we can roughly divide the processes of AVM formation in three phases; initiation, maturation, and maintenance (detailed in **Figure S1** legend**)**. In order to investigate whether the VEGF blockade affects only the formation of AVMs at the initiation phase or also the maturation and/or maintenance of established AVMs at the subsequent phases, G6.31 was topically applied directly on the window chamber at various phases. In the saline-treated group (n=5), the typical process of AVM

formation and vascular remodeling occurred as described above (**Figure 4A, S9A and S10**). For testing the effect on the initiation phase, G6.31 was applied on day 1 and day 4 post-TM injection (n=5). Overall, the angiogenic responses appeared to be suppressed, and only a small number of AV shunts around the wound were observed (**Figure 4B, S9B**, **Figures S11**). Density of vessels containing arterial blood and vessels dilatation are markedly reduced from day 3 to the end of the imaging day (**Figure 4F**), compared to saline-injected controls, suggesting that the VEGF blockade is effective for inhibiting initiation of AV shunts.

For evaluating the effect at the maturation phase, G6.31 was applied on day 4 (n=6) or 5 (n=6), when initial AV shunts were established (**Figures 4C andD, S9C and D** and **S12 and 13**). The maturation process of AV shunts was appeared to be ceased, resulting in decreased the total number of AV shunts and the density of vessels containing arterial blood in the subsequent days (**Figure 4F**). Some AV connections failed to mature and were regressed, probably due to constriction or atresia of feeding arteries (**Figure 4D and S13**). When G6.31 was applied on day 7 (n=5) after mature AVMs and vessel remodeling manifested, enlarged major AV shunts were largely unaffected, but small and intermediate stages of AVMs appeared to be regressed (**Figures 4E, S9E**, and **S15**).

We have previously shown that mucocutaneous AVM development in adult requires two factors: genetic predisposition (i.e. *Alk1*-deficiency) and secondary factors such as wounding. *Alk1*-deficient ECs tend to migrate or sprout more in response to angiogenic stimuli [26], and inhibition of ALK1 signaling increased vascular density in the developing retina [27, 28]. This characteristic is perhaps related to down-regulations of arterial marker genes, including Notch pathway genes [27-29]. The vascular density of control and *Alk1*-iKO in response to wound was not significantly different in the initiation phases (Days 1-3). It appeared to be higher in *Alk1*-iKO compared to controls from Day4, but this difference might be due to dilation of vessels rather than increase of vascular branches (**Figure S15**).

We show here that angiogenesis is a vital component among the wound effects, and AV shunts develop from nascent blood vessels during active angiogenesis. Therefore, inhibition of angiogenesis can be an effective therapy for prevention of AVM development. Bevacizumab nasal spray is an emerging therapeutic application for epistaxis on HHT patients [7-9, 30]. However, there is a paucity of evidence on how the VEGF blockade affects AVMs. Recently, Ardelean *et al* have utilized G6.31 on *Eng*- and *Alk1*-heterozygous mice to evaluate the VEGF bloackade on lung and liver vasculature [31], but they could not evaluate it in the perspective of AVM formation. We showed here direct *in vivo* evidence that VEGF blockade not only affects the initiation of AVMs but also maturation and even maintenance of established AV shunts, providing a better scientific basis for the therapeutic effect of VEGF blockades for epistaxis and GI bleeding in HHT patients. We speculate that VEGF blockades may normalize hyper-response to angiogenic stimuli in *Alk1*-deficient endothelial cells [26] and also constrict feeding arteries for the initiation and maturation of AVMs. Although the hyperspectral imaging is instrumental to localize the early events of AV shunts, the current system has limitation to obtain detail information regarding molecular and cellular basis which leads to AV shunt. Additional imaging modality having higher resolutions, deeper axial penetration, and hemodynamics coupled with the spectral

imaging system would allow us to overcome the limitations, The presented experimental model is an invaluable system for precise molecular mechanism of action of VEGF blockades as well as for preclinical screening of drug candidates for epistaxis and GI bleedings.

Methods

All *in vivo* procedures were conducted in accordance with animal use guidelines established by the University of Florida Institutional Animal Care and Use Committee. Full methods and any associated references are available in “Supplementary Methods”.

Supplementary Material

Refer to Web version on PubMed Central for supplementary material.

Acknowledgments

We thank Genentech (Roche) for providing G6.31 antibodies. This work is supported by NIH grant HL64024 (S.P.O), HHT foundation international Inc (S.P.O), and AHA predoctoral fellowship (Y.H.K.).

References

1. Shovlin CL. Hereditary haemorrhagic telangiectasia Pathophysiology, diagnosis and treatment. Blood Reviews. 2010; 24:203–219. [PubMed: 20870325]
2. Abdalla SA, Letarte M. Hereditary haemorrhagic telangiectasia: current views on genetics and mechanisms of disease. J Med Genet. 2006; 43:97–110. [PubMed: 15879500]
3. Johnson DW, Berg JN, Baldwin MA, Gallione CJ, Marondel I, Yoon SJ, Stenzel TT, Speer M, Pericak-Vance MA, Diamond A, Guttmacher AE, Jackson CE, Attisano L, Kucherlapati R, Porteous ME, Marchuk DA. Mutations in the activin receptor-like kinase 1 gene in hereditary haemorrhagic telangiectasia type 2. Nat Genet. 1996; 13:189–195. [PubMed: 8640225]
4. McAllister KA, Grogg KM, Johnson DW, Gallione CJ, Baldwin MA, Jackson CE, Helmbold EA, Markel DS, McKinnon WC, Murrell J. Endoglin, a TGF-beta binding protein of endothelial cells, is the gene for hereditary haemorrhagic telangiectasia type 1. Nat Genet. 1994; 8:345–351. [PubMed: 7894484]
5. Fleetwood IG, Steinberg GK. Arteriovenous malformations. Lancet. 2002; 359:863–873. [PubMed: 11897302]
6. Letteboer TG, Mager HJ, Snijder RJ, Lindhout D, Ploos van Amstel HK, Zanen P, Westermann KJ. Genotype-phenotype relationship for localization and age distribution of telangiectases in hereditary hemorrhagic telangiectasia. Am J Med Genet A. 2008; 146A:2733–2739. [PubMed: 18831062]
7. Karnezis TT, Davidson TM. Efficacy of Intranasal Bevacizumab (Avastin) Treatment in Patients with Hereditary Hemorrhagic Telangiectasia-Associated Epistaxis. Laryngoscope. 2011; 121:636–638. [PubMed: 21344445]
8. Karnezis TT, Davidson TM. Treatment of hereditary hemorrhagic telangiectasia with submucosal and topical bevacizumab therapy. Laryngoscope. 2012; 122:495–497. [PubMed: 22147664]
9. Simonds J, Miller F, Mandel J, Davidson TM. The Effect of Bevacizumab (Avastin) Treatment on Epistaxis in Hereditary Hemorrhagic Telangiectasia. Laryngoscope. 2009; 119:988–992. [PubMed: 19194865]
10. Dupuis-Girod S, Ginon I, Saurin JC, Marion D, Guillot E, Decullier E, Roux A, Carette MF, Gilbert-Dussardier B, Hatron PY, Lacombe P, Lorcerie B, Riviere S, Corre R, Giraud S, Bailly S, Paintaud G, Ternant D, Valette PJ, Plauchu H, Faure F. Bevacizumab in Patients With Hereditary Hemorrhagic Telangiectasia and Severe Hepatic Vascular Malformations and High Cardiac Output. Jama-Journal of the American Medical Association. 2012; 307:948–955.

11. Hoag JB, Terry P, Mitchell S, Reh D, Merlo CA. An Epistaxis Severity Score for Hereditary Hemorrhagic Telangiectasia. Laryngoscope. 2010; 120:838–843. [PubMed: 20087969]
12. Park SO, Wankhede M, Lee YJ, Choi EJ, Fliess N, Choe SW, Oh SH, Walter G, Raizada MK, Sorg BS, Oh SP. Real-time imaging of de novo arteriovenous malformation in a mouse model of hereditary hemorrhagic telangiectasia. Journal of Clinical Investigation. 2009; 119:3487–3496. [PubMed: 19805914]
13. Walker EJ, Su H, Shen FX, Choi EJ, Oh SP, Chen G, Lawton MT, Kim H, Chen YM, Chen WQ, Young WL. Arteriovenous Malformation in the Adult Mouse Brain Resembling the Human Disease. Annals of Neurology. 2011; 69:954–962. [PubMed: 21437931]
14. Lopez-Novoa JM, Bernabeu C. The physiological role of endoglin in the cardiovascular system. American Journal of Physiology-Heart and Circulatory Physiology. 2010; 299:H959–H974. [PubMed: 20656886]
15. Corti P, Young S, Chen CY, Patrick MJ, Rochon ER, Pekkan K, Roman BL. Interaction between alk1 and blood flow in the development of arteriovenous malformations. Development. 2011; 138:1573–1582. [PubMed: 21389051]
16. Sorg BS, Moeller BJ, Donovan O, Cao Y, Dewhirst MW. Hyperspectral imaging of hemoglobin saturation in tumor microvasculature and tumor hypoxia development. J Biomed Opt. 2005; 10:44004. [PubMed: 16178638]
17. Sorg BS, Hardee ME, Agarwal N, Moeller BJ, Dewhirst MW. Spectral imaging facilitates visualization and measurements of unstable and abnormal microvascular oxygen transport in tumors. J Biomed Opt. 2008; 13:014026. [PubMed: 18315384]
18. Danhier F, Ansorena E, Silva JM, Coco R, Le Breton A, Preat V. PLGA-based nanoparticles: An overview of biomedical applications. Journal of Controlled Release. 2012; 161:505–522. [PubMed: 22353619]
19. Acharya AP, Clare-Salzler MJ, Keselowsky BG. A high-throughput microparticle microarray platform for dendritic cell-targeting vaccines. Biomaterials. 2009; 30:4168–4177. [PubMed: 19477505]
20. Mattsbybaltzer I, Jakobsson A, Sorbo J, Norrby K. Endotoxin Is Angiogenic. International Journal of Experimental Pathology. 1994; 75:191–196. [PubMed: 7522030]
21. Ramanathan M, Pinhal-Enfield G, Hao I, Leibovich SJ. Synergistic up-regulation of vascular endothelial growth factor (VEGF) expression in macrophages by adenosine A(2A) receptor agonists and endotoxin involves transcriptional regulation via the hypoxia response element in the VEGF promoter. Molecular Biology of the Cell. 2007; 18:14–23. [PubMed: 17065555]
22. Xiong M, Elson G, Legarda D, Leibovich SJ. Production of vascular endothelial growth factor by murine macrophages - Regulation by hypoxia, lactate, and the inducible nitric oxide synthase pathway. American Journal of Pathology. 1998; 153:587–598. [PubMed: 9708818]
23. Campa C, Kasman I, Ye W, Lee WP, Fuh G, Ferrara N. Effects of an anti-VEGF-A monoclonal antibody on laser-induced choroidal neovascularization in mice: optimizing methods to quantify vascular changes. Invest Ophthalmol Vis Sci. 2008; 49:1178–1183. [PubMed: 18326747]
24. Schonthaler HB, Huggenberger R, Wculek SK, Detmar M, Wagner EF. Systemic anti-VEGF treatment strongly reduces skin inflammation in a mouse model of psoriasis. Proceedings of the National Academy of Sciences of the United States of America. 2009; 106:21264–21269. [PubMed: 19995970]
25. Walker EJ, Su H, Shen FX, Degos V, Jun K, Young WL. Bevacizumab Attenuates VEGF-Induced Angiogenesis and Vascular Malformations in the Adult Mouse Brain. Stroke. 2012; 43:1925–1930. [PubMed: 22569934]
26. Choi EJ, Kim YH, Choe SW, Tak YG, Garrido-Martin EM, Chang M, Lee YJ, Oh SP. Enhanced Responses to Angiogenic Cues Underlie the Pathogenesis of Hereditary Hemorrhagic Telangiectasia 2. Plos One. 2013:8.
27. Ricard N, Ciais D, Levet S, Subileau M, Mallet C, Zimmers TA, Lee SJ, Bidart M, Feige JJ, Bailly S. BMP9 and BMP10 are critical for postnatal retinal vascular remodeling. Blood. 2012; 119:6162–6171. [PubMed: 22566602]

28. Larrivee B, Prahst C, Gordon E, del Toro R, Mathivet T, Duarte A, Simons M, Eichmann A. ALK1 Signaling Inhibits Angiogenesis by Cooperating with the Notch Pathway. Developmental Cell. 2012; 22:489–500. [PubMed: 22421041]

29. Kim JH, Peacock MR, George SC, Hughes CCW. BMP9 induces EphrinB2 expression in endothelial cells through an Alk1-BMPRII/ActRII-ID1/ID3-dependent pathway: implications for hereditary hemorrhagic telangiectasia type II. Angiogenesis. 2012; 15:497–509. [PubMed: 22622516]

30. Davidson TM, Olitsky SE, Wei JL. Hereditary Hemorrhagic Telangiectasia/Avastin. Laryngoscope. 2010; 120:432–435. [PubMed: 19998344]

31. Ardelean DS, Jerkic M, Yin M, Peter M, Ngan B, Kerbel RS, Foster FS, Letarte M. Endoglin and activin receptor-like kinase 1 heterozygous mice have a distinct pulmonary and hepatic angiogenic profile and response to anti-VEGF treatment. Angiogenesis. 2014; 17:129–146. [PubMed: 24061911]

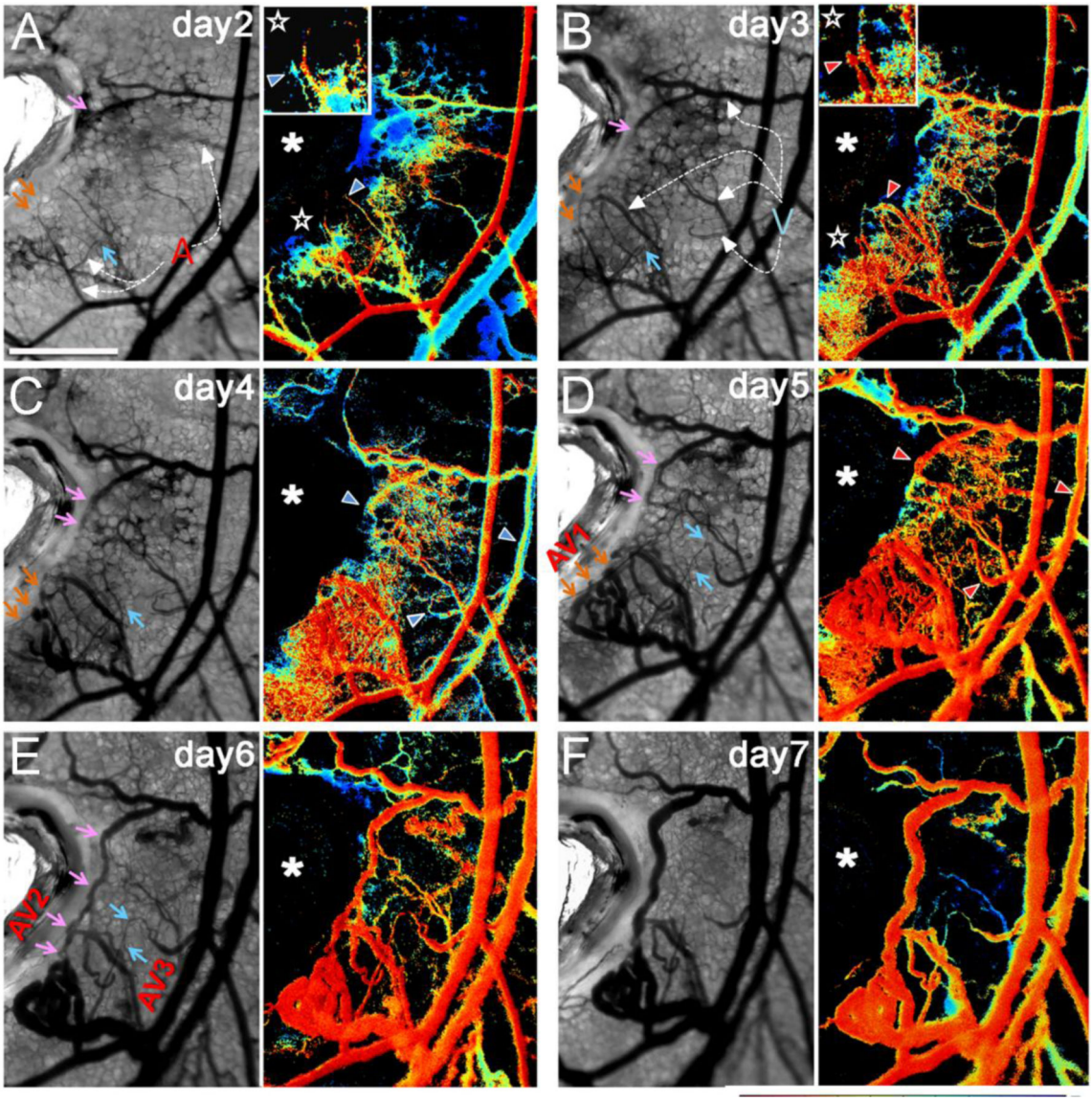

Figure 1.

Development of AVMs involves novel connections between nascent arteries and veins. **A-F.** Brightfield intravital images and corresponding hyperspectral images of the wound area in the dorsal window chamber from day 2 to day 7 after TM administration and wounding show how AVMs develop in the *R26*$^{CreER/+}$;*Alk1*$^{2f/2f}$ mice. Arterial (A) and venous (V) branches can be distinguished by spectral images and are indicated by white arrows with dotted lines (**A** and **B**). Three arterio-venous (AV) fistulae are indicated by AV1-3. Growth and remodeling of vessels involved in AV shunts are indicated by colored arrows. Arterial blood flowing into venous branches through AV shunts could be detected. Changes of hemoglobin saturation (Hb_{sat}) status in venous branchs are indicated by blue (low Hb_{sat}) and red (high Hb_{sat}) arrowheads. AV1 (orange arrows) was developed from connections between a couple of arterial branches and multiple neighboring venous branches (**A-D**). Insets in **A** and **B** are the magnified views of the areas indicated by stars. AV2 (pink arrows) developed as a venous branch extended to AV1 (**BE**). AV3 (blue arrows) established by an

extension of a artery to a venous branch (**B-E**). Wound sites are indicated by asterisks. All images are in the same magnification, and the scale bar indicates 500 m. The color bar in the bottom of panel F indicates Hb saturation levels.

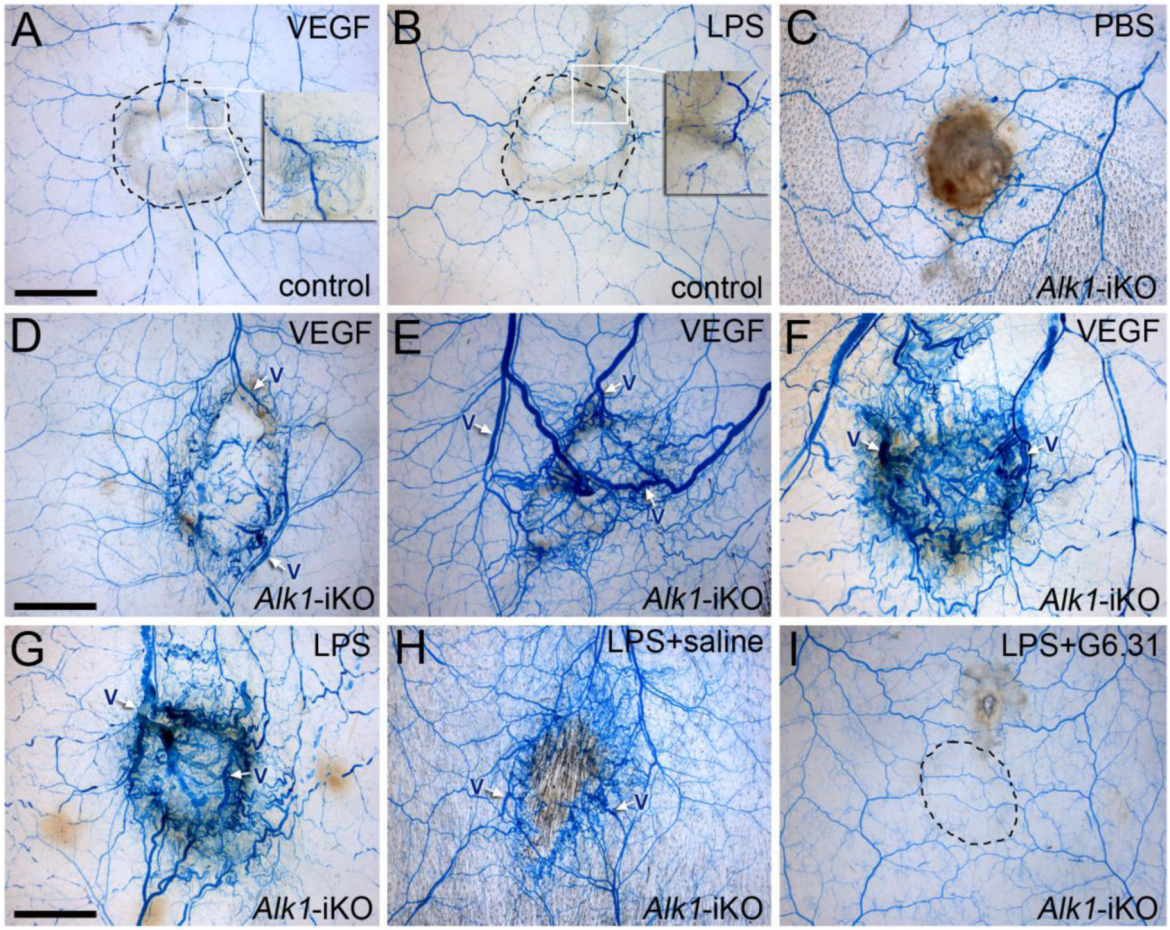

Figure 2.

Angiogenic stimulation can mimic the wound effect for the development of skin AVMs in *Alk1*-deficient adult subdermal vessels. VEGF, LPS or PBS encapsulated in PLGA particles were implanted under dorsal skin of TM-injected *Alk1*-iKO mice. Subdermal blood vessels containing latex dye infused via left heart were visualized after clearing in the organic solvents. **A**-**C**, VEGF- or LPS-PLGA on control mice (**A**, **B**; n=3 for each condition), or PBSPLGA on *Alk1*-iKO mice (**C**, n=8) did not induce AVMs. **D**-**G**, VEGF-PLGA (**D**-**F**, n=4) or LPS-PLGA (**G**, n=5) mimicked the wound effect on the formation of AVMs. **H**-**I**, LPS-PLGA on saline-treated *Alk1*-iKO mice induced AVMs (**H**, n=5), but not on G6.31-treated mice (**I**, n=3). Dotted circles indicate the areas of PLGA particles. Scale bars indicate 4 mm.

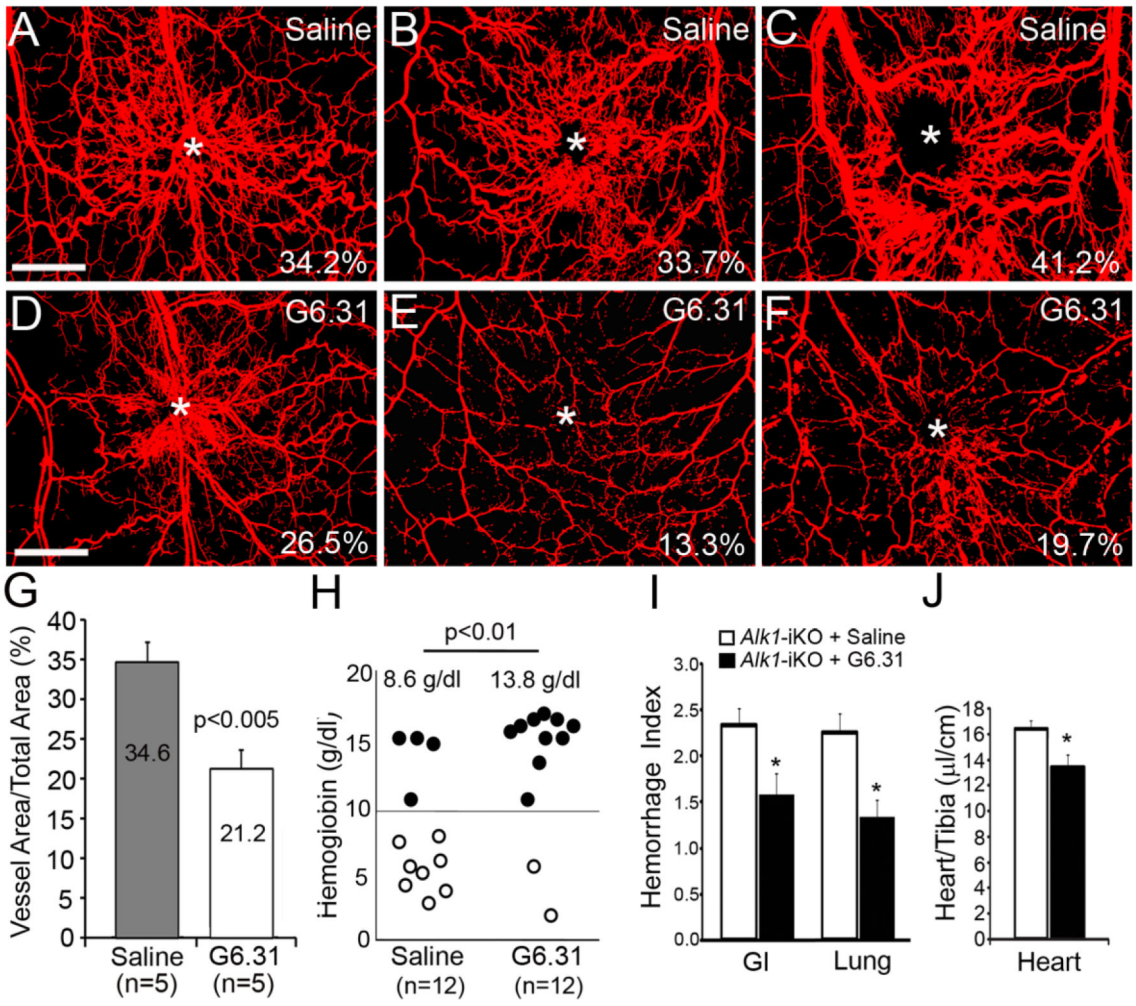

Figure 3.

VEGF neutralizing antibody suppressed wound-induced AVM formation and visceral hemorrhage in *Alk1*-deficient adult mice. **A**-**F**, Processed images of subdermal blood vessels containing latex dye (**Figure S5**). Saline (**A**-**C**, n=12) or G6.31 (**D**-**F**, n=12) were intraperitoneally injected into *Alk1*-iKO adult mice 1 and 4 days after TM treatment and incisional wounding on dorsal skin. Latex dye was perfused via left heart on day 9. Wound sites are indicated by asterisks, and percentages of area covered by blood vessels containing latex dye are indicated in each panel. Scale bars in each panel indicate 2 mm. **G**, Histogram showing a significant reduction of the percentage of vessel area in G6.31-treated group (n=5) compared to that in the saline-treated group (n=5). **H**, Hemoglobin (Hb) concentration was measured in saline-treated (n=12) and G6.31-treated (n=12) *Alk1*-deficient mice 9 days after TM treatment. Each dot indicates Hb level of an individual mouse. Hb level higher than 10 g/dl is shown by filled dots. **I**, Severity of GI and lung bleeding was expressed as a severity index based on visual inspection and categorization (n=12, each group). **J**, Heart enlargement related to hemorrhaging in *Alk1*-deficient mice (n=12, each group) was expressed as a ratio of heart volume and tibia length (l/cm). * indicates a significant difference ($p<0.05$) vs. saline-treated control.

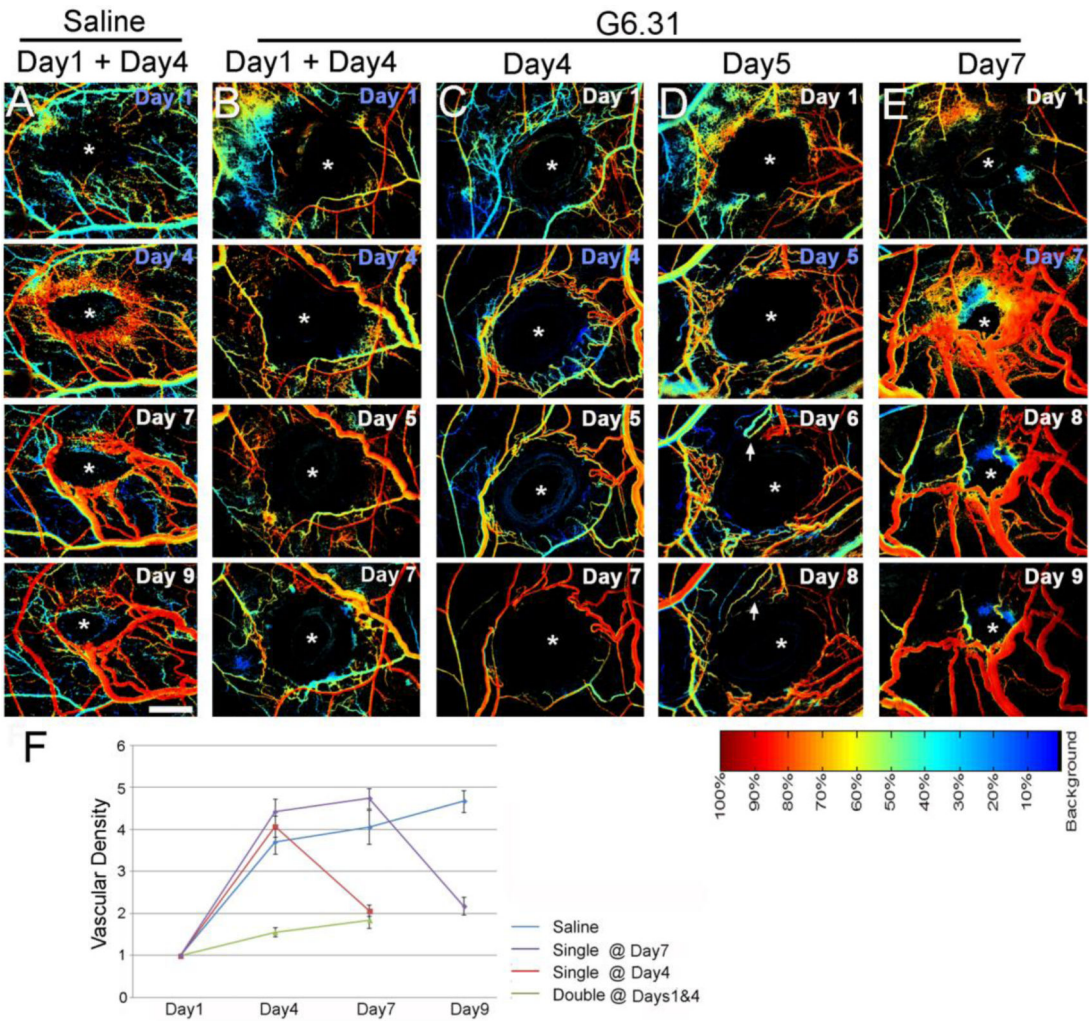

Figure 4.

VEGF-neutralizing antibody can prevent and normalize wound-induced AVMs formed at various stages in *Alk1*-deficient adult mice. Saline (**A**, n=5) or G6.31 (**B**-**E**) were directly injected into the window chamber of the *Alk1*-iKO adult mice twice (day 1 and day 4; **B**, n=5) or once [day 4 (**C**, n=6), day 5 (**D**, n=6) or day 7 (**E**, n=5)] after TM treatment and incisional wounding on dorsal skin. Disappearance of AV shunts, hemodynamic changes, and regression of established AVMs after G6.31 treatment were monitored daily through hyperspectral images. S and G6 indicate the day of saline and G6.31 antibody injection, respectively. White arrows in days 6 and 8 of single injection on day 5 indicate the vessels where AV shunt is resolved. The wound areas are marked by asterisks. Daily spectral images are shown in **Figure S10**, and full spectral and corresponding bright field images are shown in F**igures S11-S15**. All images are in the same magnification, and the scale bar indicates 1 mm. **F**, Severity of AVMs was expressed as vascular density (percentage of vessel area containing arterial blood/total vessel area).